Science Bulletin 63 (2018) 1118–1124

Contents lists available at ScienceDirect

Science Bulletin

journal homepage: www.elsevier.com/locate/scib

Article

Fast response CdS-CdS_xTe_{1-x}-CdTe core-shell nanobelt photodetector

Mingwei Tang [a], Pengfei Xu [b], Zhong Wen [a], Xing Chen [c], Chenlei Pang [a], Xuechu Xu [a], Chao Meng [a], Xiaowei Liu [a], He Tian [c], Nagarajan Raghavan [d], Qing Yang [a,e,*]

[a] State Key Laboratory of Modern Optical Instrumentation, College of Optical Science and Engineering, Zhejiang University, Hangzhou 310027, China
[b] The Fifth Research Institute of Ministry of Industry and Information Technology (MIIT), Guangzhou 510610, China
[c] Center of Electron Microscopy, Zhejiang University, Hangzhou 310027, China
[d] Engineering Product Development (EPD) Pillar, Singapore University of Technology and Design, Singapore 487372, Singapore
[e] Collaborative Innovation Center of Extreme Optics, Shanxi University, Taiyuan 030006, China

ARTICLE INFO

Article history:
Received 2 May 2018
Received in revised form 6 July 2018
Accepted 30 July 2018
Available online 4 August 2018

Keywords:
CdS-CdS_xTe_{1-x}-CdTe
Core-shell
Photodetector
Fast response

ABSTRACT

Quasi-one-dimensional semiconductor nanostructure-based photodetectors show high sensitivity but suffer from slow response speed due to surface reaction. Here, we report a fast-response CdS-CdS_xTe_{1-x}-CdTe core-shell nanobelt photodetector with a rise time of 11 μs, which is the fastest among CdS based photodetectors reported previously. The improved response speed is ascribed to the suppressed possibilities of surface reaction resulting from the core-shell structure and heterojunction among the CdS, CdS_xTe_{1-x} and CdTe. The measured response spectrum of CdS-CdS_xTe_{1-x}-CdTe core-shell nanobelt photodetector covers a wide range from 355 to 785 nm. Moreover, high responsivity (1,520 A/W) and large 3 dB bandwidth (~22.9 kHz) are obtained along with the fast response. The high performance in responsivity, sensitivity, spectral response and photoresponse speed makes this device a promising candidate for practical application in optical sensing, communication and imaging.

1. Introduction

One-dimensional (1D) nano-photodetectors have proved to be very promising for photodetection in integrated opto-electric circuits and systems [1]. Compared with traditional thin-film photodetectors, 1D nanostructures have larger surface-to-volume ratio, smaller size and higher carrier mobility, and thus tend to exhibit higher sensitivity and larger internal gain [2–6], which makes them promising candidates in practical applications such as optical communication, imaging and single photon detecting [7–9]. Thanks to the development of nano fabrication method [10–15], pure nanowires (NWs)/nanobelts (NBs) with high quality have been fabricated successfully [16–20]. However, for pure NWs/NBs based photodetectors, fast photoresponse speed and high sensitivity cannot be achieved simultaneously for the positive correlation between sensitivity and characteristic lifetime according to existing studies [7,21].

Here we report a highly sensitive, fast response nano-photodetector based on a single CdS-CdS_xTe_{1-x}-CdTe core-shell NB. The core-shell NBs are fabricated using vapor-liquid-solid (VLS) method. As-fabricated NB was deposited on a SiO_2 substrate and followed by the fabrication of metal contacts on both ends of the NB. As a result, the typical rise and fall time of our CdS-CdS_xTe_{1-x}-CdTe NB photodetector are 11 and 23 μs, respectively. Compared with pure CdS photodetector studied under the same conditions (same biased voltage and illumination density), experimental results indicate that this novel photodetector exhibits superior performances than CdS NB photodetector in response speed, sensitivity as well as responsivity.

2. Experimental

To synthesize CdS-CdS_xTe_{1-x}-CdTe core-shell NBs, a two-step thermal deposition method using a source/substrate-movable chemical vapor deposition (CVD) system was adopted [22–24]. First, 0.5 g of CdS powder and CdTe powder in two alumina crucibles were placed in the center and edge of the quartz tube. After vacuumized to ~1 mbar (1 mbar = 100 Pa), the furnace was heated up from room temperature to around 850 °C at a rate of ~40 °C/min and kept at 850 °C for about 60 min. Second, alumina crucible containing CdTe powder was transferred into heating zone of the furnace and kept for about 12–20 min before cooling down to room temperature. During the whole process, substrates were placed downstream in the tube under a constant flow of nitrogen

* Corresponding author.
E-mail address: qingyang@zju.edu.cn (Q. Yang).

https://doi.org/10.1016/j.scib.2018.08.003
2095-9273/

atmosphere with a flow rate of 175 sccm (standard-state cm^3/min) and a pressure of 400 mbar. Scanning electron microscope (SEM) image in Fig. 1a shows the belt-like geometry of the nanostructure with a thickness of around 50 nm. When excited by a 355-nm-wavelength pulse laser, core-shell structure of the as-fabricated NB was obviously demonstrated by its fluorescence image (Fig. 1b). Meanwhile, its photoluminescence (PL) was recorded by a spectrometer and shown in Fig. 1c. The narrow peak at 517 nm is assigned to band-edge luminescence arising from the recombination of excitons [25] in CdS, while the broad peak centered at 644 nm with a full width at half maximum (FWHM) of 119.2 nm comes from the introduction of CdTe and trap/surface states [26]. The core-shell structure was confirmed by field-emission transmission electron microscope (FE-TEM).

Fig. 2a is the high-angle angular dark field (HAADF) image of the NB and the two-dimensional (2D) elemental distribution of cadmium (Cd), sulphur (S) and tellurium (Te). The energy dispersive spectra (EDS) is shown in Fig. 2b. Fig. 2c is the EDS line scan profile across the entire NB along the line in Fig. 2a, which demonstrates that Te distributes at the edge of the NB, S distributes in the core while Cd distributes uniformly along the whole NB, indicating a CdS core and CdTe shell structure. The element Te and S coexist at the edge of the nanobelt with a thickness of about 90 nm. The high resolution transmission electron microscope (HRTEM) image taken from the side of a single CdS-CdS_xTe_{1-x}-CdTe NB has been presented in Fig. 2d, which shows that the lateral region is amorphous CdTe while the vicinity region is high-quality single crystal CdS_xTe_{1-x} structure, the central region is crystal CdS structure. The interplanar *d*-spacings of 0.353 and 0.662 nm corresponds to the (1 0 0) and (0 0 1) lattice planes. Comparing with hexagonal CdS phase (JCPDS No. 77-2306), the *d*-spacings have a little variation, which is a result of the forming of ternary crystal CdS_xTe_{1-x} alloy [24,27]. The parameter *x* defined as the S mole fraction could be determined from Fig. 2c at the edge of the nanobelt, which is about 0.909. It is worth noting that this mole ratio increases gradually from the edge to center of the NB.

The experimental setup for characterization of NB photodetectors is presented in Fig. 3. A 405-nm-wavelength laser is modulated by a function generator (DS345) and then coupled to a microscope (ZEISS Imager A2m) for excitation of photodetectors. A 10/90 (R/T) beam splitter is used to direct part of the light to an optical power meter as a reference beam for monitoring the excitation density on the CdS-CdS_xTe_{1-x}-CdTe NB. To obtain a uniform light spot, a frosted glass and a diaphragm are used. The relationship between the power illuminating on the NBs and the reference power was calibrated, which is about 1.3 in our system. The NB is in series connecting with a standard 43 KΩ resistance and the voltage on the resistance is measured by an oscilloscope. This resistance ($\sim 10^4$ Ω) was chosen for a balance of the intensity of detected signal and the auxiliary response time. The photodetector was fabricated by using silver paste to fix two ends of NB onto the SiO_2 substrate. The silver pastes also serve as the source and drain electrodes. In our work, both CdS-CdS_xTe_{1-x}-CdTe core-shell NB photodetectors and single crystalline CdS NB photodetectors were fabricated. Their electrical and optical performances are compared, such as response time, responsibility as well as sensitivity.

3. Results and discussion

The response times of CdS and CdS-CdS_xTe_{1-x}-CdTe core-shell NB photodetectors at working voltage of 5 V are presented in Fig. 4a and b. The presented photoresponse is highly stable and reproducible. With increasing light density from 0.18 to 405 mW/cm^2, both CdS and CdS-CdS_xTe_{1-x}-CdTe core-shell NB photodetectors show increasing photocurrents. However, when light turns off, pure CdS-based photodetector exhibits a much slower recovery speed. As shown in the inset of Fig. 4b, CdS-CdS_xTe_{1-x}-CdTe core-shell NB photodetector indicates a much faster rise and fall time (defined as the time of the photocurrent between 10% and 90% of the saturation value) of 11 and 23 μs. This photoresponse is much faster than that of CdS NB photodetector, which are 16 and 397 μs, respectively. Considering the auxiliary response time of the series resister, the real response time could be even shorter than this result. The photoresponse speed of this photodetector has surpassed that of the fastest CdS photodetectors reported previously [18]. In addition, CdS-CdS_xTe_{1-x}-CdTe core-shell NB photodetector has a much lower dark current compared with CdS NB photodetector, especially after high density light illumination. To further identify the response time of the CdS-CdS_xTe_{1-x}-CdTe core-shell NB photodetector, a 355-nm-wavelength pulsed laser (repetition frequency: 10 kHz, pulse width: 7 ns) was used as the light source. The time resolved photoresponse is shown in Fig. 4c. To estimate the photoresponse time, we zoom one of the pulses as demonstrated in Fig. 4d, which shows a rise and fall time of 6.6 and 14.6 μs, respectively. Since the pulse width of the laser is about several ns (much less than the response time of our device), the response time is completely determined by the intrinsic response time of our device. The excellent response speed indicates that this CdS-CdS_xTe_{1-x}-CdTe

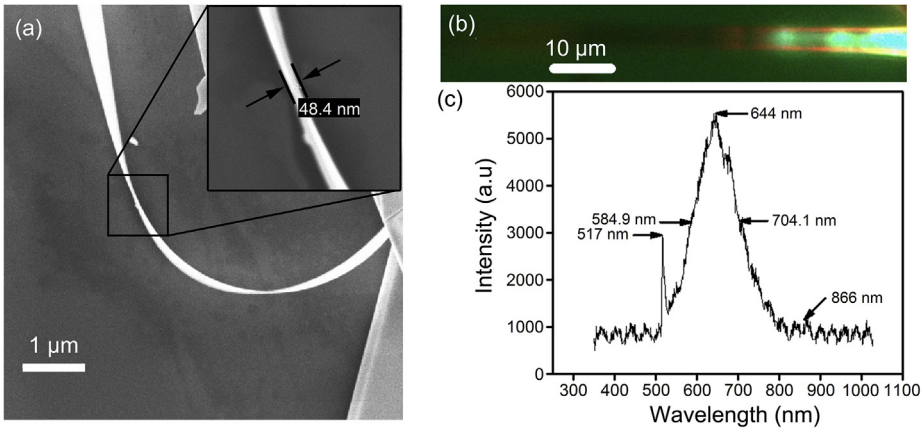

Fig. 1. (Color online) SEM and the photoluminescence analysis of the fabricated NBs. (a) SEM image of CdS-CdS_xTe_{1-x}-CdTe core-shell NBs with a thickness of about 50 nm. (b) Optical microscope image of CdS-CdS_xTe_{1-x}-CdTe NBs excited by 355-nm-wavelength laser. Emission light is filtered by a 600-nm long-pass optical filter. (c) Typical PL spectra of CdS-CdS_xTe_{1-x}-CdTe core-shell NBs.

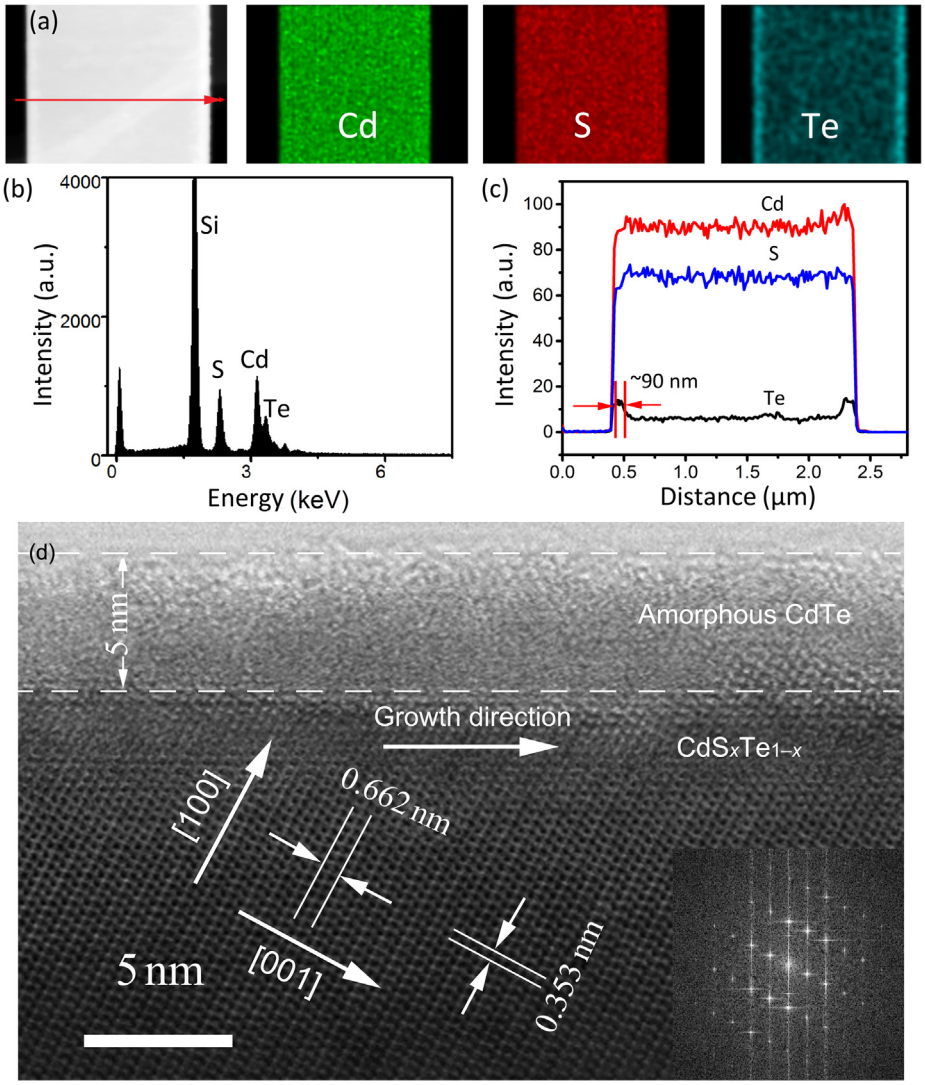

Fig. 2. (Color online) TEM analysis of the as-fabricated NBs. (a) HAADF image of the CdS-CdS_xTe_{1-x}-CdTe NB and 2D element distribution of Cd, S and Te. EDS (b) and EDS line scan profile (c) of Cd, S and Te along the line in panel (a). (d) HRTEM image taken from the side of a single core-shell NB. Inset: fast Fourier transform (FFT) analysis.

core-shell NB photodetector has the potential for fast signal detection.

Typical responsivity and sensitivity of CdS-CdS_xTe_{1-x}-CdTe core-shell NB photodetector are shown in Fig. 5. Fig. 5a exhibits typical *I-V* curve of the CdS-CdS_xTe_{1-x}-CdTe core-shell NB photodetector in the dark condition and under illumination of 405-nm-wavelength laser of different light intensity from 7.2×10^{-5} to 2.28×10^{-3} W/cm^2. Notably, the absolute current increases from 0.05 nA (dark current) to 5.8 nA (7.2×10^{-5} W/cm^2) and further to 202.6 nA (2.28×10^{-3} W/cm^2) at a working voltage of 2 V. The dependence of photocurrent on an incident optical intensity is demonstrated in Fig. 5b. Photocurrent I_{ph} and light intensity P can be fitted with a simple power law:

$$I_{ph} = 98.81P^{0.88}, \quad (1)$$

where the exponent of 0.88 close to 1 indicates the low density of trap states in the energy band of the NB [28].

Responsivity, sensitivity and external quantum efficiency (EQE) are important parameters to determinate the capability of a photodetector. These parameters can be defined as:

$$R = \frac{I_{ph}}{\phi_s}, \quad (2)$$

$$EQE = R\left(\frac{hv}{q}\right), \quad (3)$$

$$Sensitivity = (I_{light} - I_{dark})/I_{dark}, \quad (4)$$

where R is the responsivity, ϕ_s is the light power incident on the photodetector, h is the Planck's constant, v is the frequency of the light, q is the electronic charge, I_{light} and I_{dark} represent the light current and dark current, respectively. The sensitivity in Fig. 5c shows an increasing tendency and reaches over 4,075 at incident power intensity of 2.28 mW/cm^2. Remarkably, calculated responsivity of the NB photodetector extends over 550 and 1,520 A/W at incident power intensity of 2.78×10^{-7}W/cm^2 with bias voltage of 2 and 5 V, respectively. The corresponding EQE is as high as $(4.7 \times 10^5)\%$. The decrease of the responsivity with light intensity could be ascribed to the hole-trapping saturation [29].

To investigate the response time and bandwidth of our CdS-CdS_xTe_{1-x}-CdTe core-shell NB photodetector, we further increased the modulation speed step-by-step and measured photoresponse of the NB photodetector under irradiation of 405-nm-wavelength laser, with power density of 15.5 mW/cm^2. The responsivity of CdS-CdS_xTe_{1-x}-CdTe and CdS NB photodetector relative to the modulation frequency is plotted in Fig. 5d. For CdS-CdS_xTe_{1-x}-

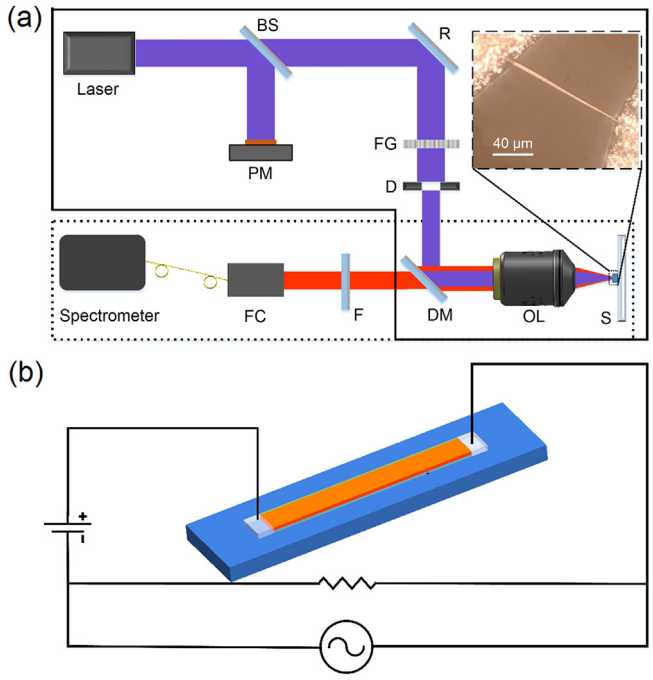

Fig. 3. (Color online) Experimental setup for photoresponse measurement and PL characterization of NB photodetectors. (a) The solid line box shows optical path for the photoresponse measurement. A 405-nm-wavelength laser is modulated by function generator as a light source. BS: 10/90 (R/T) beam splitter; PM: power meter; R: reflector; FG: frosted glass; D: diaphragm; DM: dichroic mirror; OL: objective lens; S: sample. The measurement setup of PL spectra is shown in dashed line box, a 355-nm-wavelength laser is used to excite the NBs. Generated photoluminescence is filtered and then coupled to a spectrometer. FC and F are fiber coupler and filter respectively. The microscope image of a typical CdS-CdS_xTe_{1-x}-CdTe NB photodetector is shown in the inset. (b) The circuit diagram for the NB photodetector.

CdTe core-shell NB photodetector, the responsivity keeps constant with R_0 of 10.4 A/W when the modulation frequency scales from 0 to 5 KHz and then gradually descends. The cutoff frequency, defined as the frequency when responsivity decreases by 3 dB is 22.9 kHz in this case. In contrast, the pure CdS NB photodetector shows a much smaller responsivity ($R_0 \sim 4.9$ A/W) and lower cutoff frequency (~560 Hz).

Furthermore, the detection spectrum of this newly developed device is also investigated. The spectral responses of the CdS-CdS_xTe_{1-x}-CdTe core-shell NB photodetector and CdS NB photodetector were measured from wavelength of 460 to 785 nm (Fig. 5e and f). Results show that the CdS-CdS_xTe_{1-x}-CdTe structure has a broader spectra response. For CdS NB photodetectors, the photoresponse decreases abruptly when illumination light changes from 460 to 550 nm and shows no photoresponse in the longer wavelength region because the bandgap of the CdS corresponds to a cut-off wavelength of 517 nm [18,30]. While the CdS-CdS_xTe_{1-x}-CdTe core-shell NB photodetector demonstrates a high responsivity over 100 A/W from 460 to 600 nm. Even in the longer wavelength of 650 nm, the responsivity can reach 41 A/W. The well performed photoresponse of CdS-CdS_xTe_{1-x}-CdTe core-shell NB photodetector in the long wavelength region results from the CdTe or CdS_xTe_{1-x} alloy with smaller bandgap, which indicates the successful constriction of CdS-CdS_xTe_{1-x}-CdTe core-shell structure. Fig. 5f shows the responsivity of CdS-CdS_xTe_{1-x}-CdTe core-shell NB photodetector under 785-nm-wavelength laser irradiation with different light intensity. The responsivity reaches over 4.5 A/W at the light intensity of 9×10^{-5} W/cm^2, and decreases with light power density. The overall responsivity is lower compared with that at the wavelength of 405 nm in the same power density because CdTe only takes a small portion in the alloy device, which is consistent with the EDS and HRTEM analysis in Experimental Section. As summarized in Table 1, compared with other nanostructure-based photodetectors, our CdS-CdS_xTe_{1-x}-CdTe core-shell NB photodetectors exhibit better performances such as fast response speed, high sensitivity and responsivity.

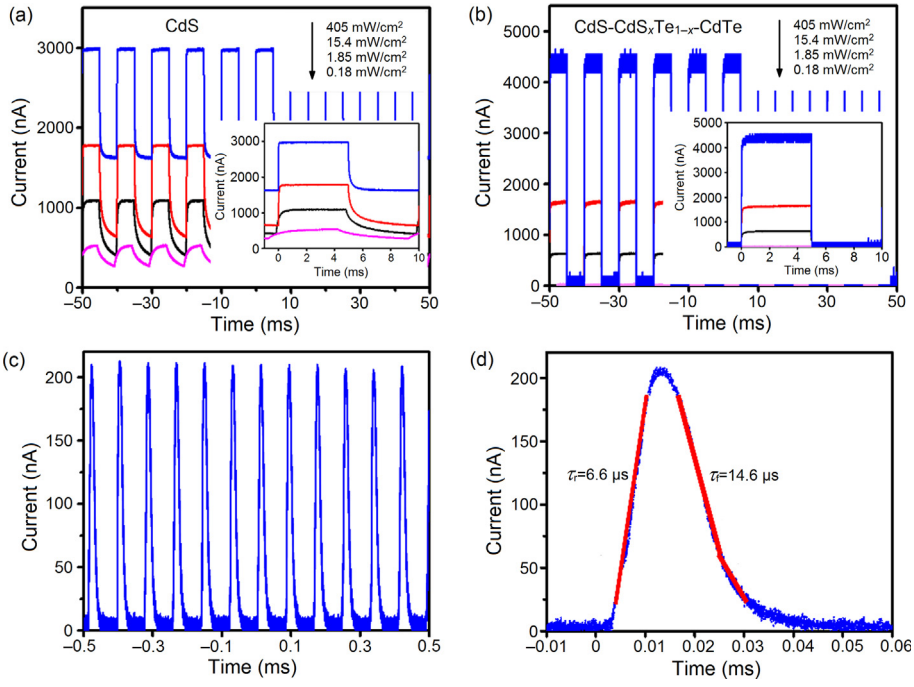

Fig. 4. (Color online) Time response of pure CdS and CdS-CdS_xTe_{1-x}-CdTe core-shell NB photodetectors. Photoresponse of pure CdS (a) and CdS-CdS_xTe_{1-x}-CdTe core-shell (b) NB photodetectors under 405-nm-wavelength laser excitation. Light modulation frequency is 100 Hz. (c) Photoresponse characteristics of CdS-CdS_xTe_{1-x}-CdTe core-shell NB photodetector under 355-nm-wavelength nanosecond pulsed laser excitation. (d) Enlarged single pulse in (c) for extraction of rise and fall time.

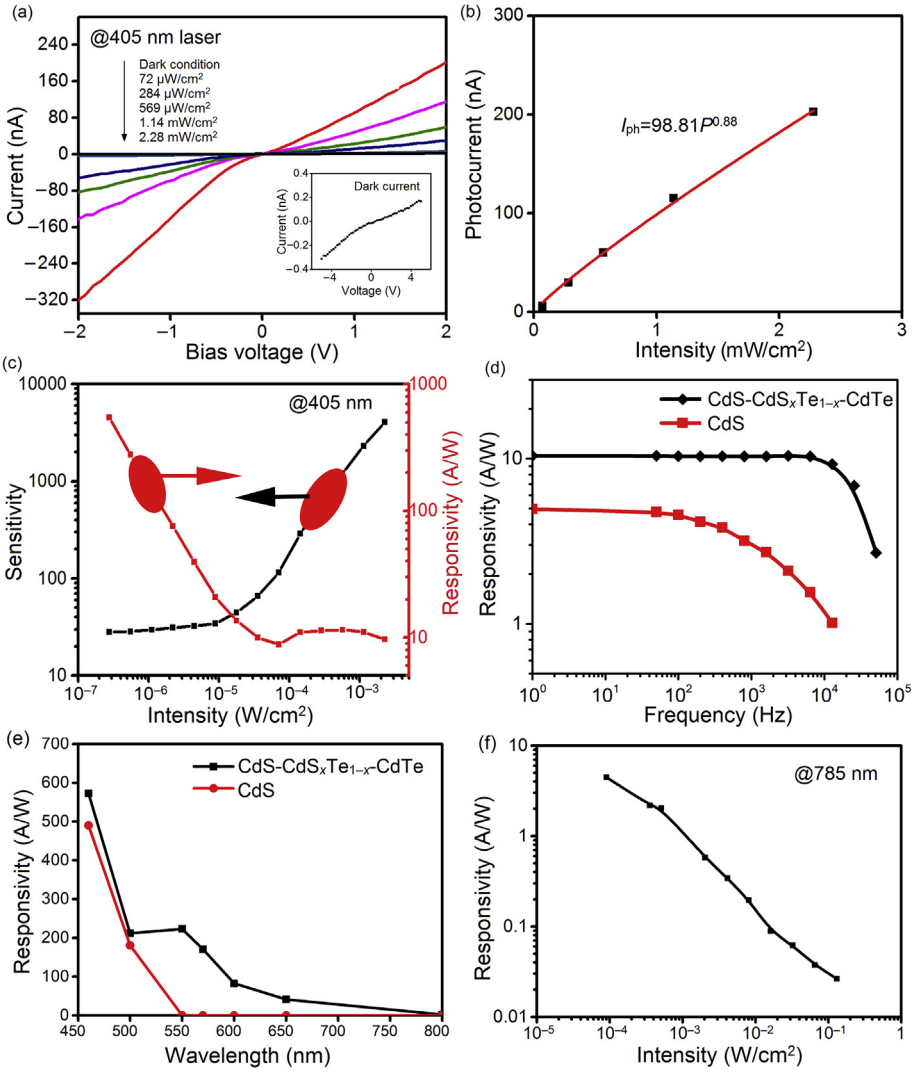

Fig. 5. (Color online) Responsivity and sensitivity of photodetectors. (a) *I-V* characteristics of single CdS-CdS$_x$Te$_{1-x}$-CdTe core-shell NB photodetector irradiated by 405-nm-wavelength laser. Inset shows the dark state *I-V* curve. (b) Photocurrent as a function of the incident light intensity at a 2 V source-drain bias voltage. (c) Dependence of sensitivity and responsivity on light intensity shown in (a). (d) Responsivity relative to modulation frequency under incident light density of 15.4 mW/cm^2 with a bias voltage of 5 V. (e) The spectral response of the CdS-CdS$_x$Te$_{1-x}$-CdTe core-shell NB and CdS NB photodetectors. (f) Responsivity of CdS-CdS$_x$Te$_{1-x}$-CdTe core-shell NB photodetector under excitation of 785-nm-wavelength laser.

To understand the improved performance of CdS-CdS$_x$Te$_{1-x}$-CdTe core-shell NB photodetector such as faster photoresponse speed and enhanced sensitivity. Here we developed a theoretical model (Fig. 6) to investigate the physical mechanism behind our CdS-CdS$_x$Te$_{1-x}$-CdTe core-shell NB photodetector. The as-fabricated CdTe [34,37] and CdS [22] nanostructures generally show the p-type and n-type characteristics. Fig. 6b shows the electron-hole pair transfer process in the CdS-CdS$_x$Te$_{1-x}$-CdTe core-shell NB. Compared with pure CdS NB photodetectors, the resistance of the core-shell NB photodetector will increase in dark condition because of depletion of carriers in the layer of CdS$_x$Te$_{1-x}$, resulting in low dark current and small noise. When light is illuminated on the photodetector, the CdS, CdS$_x$Te$_{1-x}$ and CdTe absorb photons around their bandgaps (from 1.5 to 2.4 eV) and produce photo-generated carriers. The photoelectrons will be injected from CdTe and CdS$_x$Te$_{1-x}$ to CdS core layer. At the same time, holes will be transferred from CdS to CdS$_x$Te$_{1-x}$ and then to CdTe shell layer. Because the CdTe layer in our device is much thinner that of CdS$_x$Te$_{1-x}$, the photogenerated holes will mainly transfer to the alloy layer. The separation of photo-generated carriers leads to reduced carrier recombination probability and increases the photocurrent. In addition, the radiative energy in the CdS core layer can be re-absorbed by the CdS$_x$Te$_{1-x}$ and CdTe shell layers, contributing to a higher photocurrent and responsivity of the heterostructure devices [36]. As a result of the two reasons above, the sensitivity and responsivity could be enhanced. The absorption of photons and carrier generation of CdS, CdS$_x$Te$_{1-x}$ and CdTe simultaneously contribute to a broader response spectrum compared with pure CdS and CdTe devices.

Furthermore, this core-shell structure plays an influential role in improving the photoresponse speed. For pure CdS NB-based photodetectors, the photoresponse is mainly governed by desorption and adsorption of oxygens [38]. Since the equilibrium of gas molecules interacting with carriers takes longer time, the response speed of pure nanostructure based photodetectors is limited [39,40]. In contrast, in our designed core-shell NB photodetectors, the intrinsic positive charge in CdTe shell will avoid the absorption of oxygens and thus operation of this kind NB photodetectors mainly depends on the built-in potential at the interface, which has a much faster carriers-separating speed. As a result of the

Table 1
Comparison of the characteristic parameters of CdS-CdS_xTe_{1-x}-CdTe core-shell NB photodetector and other nanostructure-based photodetectors.

Materials	Sensitivity	Responsivity (A/W)	Rise time	Fall time	Ref
CdS NW	3×10^5	2.6×10^5	12.6 ms	180 ms	[31]
CdS NB	4	7.3×10^4	~20 μs	~20 μs	[18]
CdS NB	2.7×10^6	2.0×10^2	137 μs	379 μs	[32]
CdS/Cd NW	8	NA	15 ms	15 ms	[12]
CdS/CdS:SnS2 NW	1.5×10^5	2.5×10^3	10 ms	10 ms	[33]
CdTe NW	19	80.1	0.7 s	1 s	[34]
CdSe NW	40	NA	700 ms	700 ms	[35]
Ion exchanged CdS NW	2.5×10^3	4.57	1 s	2 s	[30]
CdS-CdSe alloy NB	10^6	1.16×10^3	30 ms	90 ms	[36]
CdS-CdS_xTe_{1-x}-CdTe core-shell NB	4×10^3	1.5×10^3	11 μs	23 μs	This work

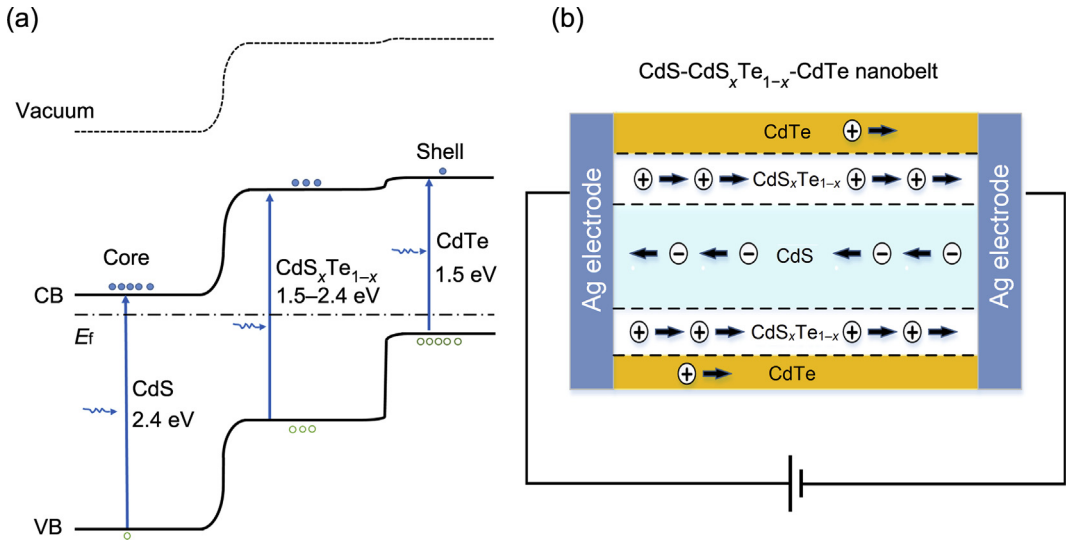

Fig. 6. (Color online) Theoretical model of CdS-CdS_xTe_{1-x}-CdTe core-shell NB photodetectors. (a) Schematic energy band diagram for CdS-CdS_xTe_{1-x}-CdTe NB under light irradiation. E_f is the Fermi level. CB and VB represent the conduction band and valence band respectively. (b) Schematic diagram of electron-hole pair separation and transfer in the CdS-CdS_xTe_{1-x}-CdTe heterostructure photodetector.

abovementioned mechanism, the responsivity and response speed of the CdS-CdS_xTe_{1-x}-CdTe core-shell NB photodetectors have been extraordinarily optimized.

4. Conclusions

In summary, a fast response CdS-CdS_xTe_{1-x}-CdTe core-shell NB based photodetector with relative high sensitivity and responsivity has been presented. The rise time and fall time of the photodetector can be as short as 11 and 23 μs. The alloyed NB photodetector also demonstrates excellent sensing capability covering the whole visible spectrum. The improved performance is ascribed to the heterostructure in CdS-CdS_xTe_{1-x}-CdTe. Since the fabrication process is simple, the CdS-CdS_xTe_{1-x}-CdTe NB photodetectors will find wide applications in optoelectronic nano devices in the fields of information, communications and environmental monitoring.

Conflict of interest

The authors declare that they have no conflict of interest.

Acknowledgments

We thank the Center of Electron Microscopy of Zhejiang University. This work was supported by the National Natural Science Foundation of China (51672245 and 61735017), the National Key Basic Research Program of China (2015CB352003), Zhejiang Provincial Natural Science Foundation of China (R17F050003), the Fundamental Research Funds for the Central Universities, the Program for Zhejiang Leading Team of S&T Innovation and the Fundamental Research Funds for the Central Universities.

References

[1] Lieber CM, Wang ZL. Functional nanowires. MRS Bull 2007;32:99–108.
[2] Yang Q, Guo X, Wang WH, et al. Enhancing sensitivity of a single ZnO micro-/nanowire photodetector by piezo-phototronic effect. ACS Nano 2010;4:6285–91.
[3] Soci C, Zhang A, Xiang B, et al. ZnO nanowire UV photodetectors with high internal gain. Nano Lett 2007;7:1003–9.
[4] Li QH, Gao T, Wang TH. Optoelectronic characteristics of single CdS nanobelts. Appl Phys Lett 2005;86:193109.
[5] Wei TY, Huang CT, Hansen BJ, et al. Large enhancement in photon detection sensitivity via Schottky-gated CdS nanowire nanosensors. Appl Phys Lett 2010;96:013508.
[6] Hu YF, Zhou J, Yeh PH, et al. Supersensitive, fast-response nanowire sensors by using Schottky contacts. Adv Mater 2010;22:3327–32.
[7] Soci C, Zhang A, Bao XY, et al. Nanowire photodetectors. J Nanosci Nanotechnol 2010;10:1430–49.
[8] Sang LW, Liao MY, Sumiya M. A comprehensive review of semiconductor ultraviolet photodetectors: from thin film to one-dimensional nanostructures. Sensors Basel 2013;13:10482–518.
[9] Hu XL, Cheng YH, Gu C, et al. Superconducting nanowire single-photon detectors: recent progress. Sci Bull 2015;60:1980–3.
[10] Yang PD, Yan HQ, Mao S, et al. Controlled growth of ZnO nanowires and their optical properties. Adv Funct Mater 2002;12:323–31.
[11] Ahn Y, Dunning J, Park J. Scanning photocurrent imaging and electronic band studies in silicon nanowire field effect transistors. Nano Lett 2005;5:1367–70.

[12] Li QG, Penner RM. Photoconductive cadmium sulfide hemicylindrical shell nanowire ensembles. Nano Lett 2005;5:1720–5.
[13] Yang Q, Sha J, Wang L, et al. MgO nanostructures synthesized by thermal evaporation. Mater Sci Eng C 2006;26:1097–101.
[14] Xia YN, Yang PD, Sun YG, et al. One-dimensional nanostructures: synthesis, characterization, and applications. Adv Mater 2003;15:353–89.
[15] Han N, Yang ZX, Shen LF, et al. Design and fabrication of 1-D semiconductor nanomaterials for high-performance photovoltaics. Sci Bull 2016;61:357–67.
[16] Calarco R, Marso M, Richter T, et al. Size-dependent photoconductivity in MBE-grown GaN-nanowires. Nano Lett 2005;5:981–4.
[17] Salfi J, Philipose U, de Sousa CF, et al. Electrical properties of ohmic contacts to ZnSe nanowires and their application to nanowire-based photodetection. Appl Phys Lett 2006;89:261112.
[18] Li L, Wu P, Fang X, et al. Single-crystalline CdS nanobelts for excellent field-emitters and ultrahigh quantum-efficiency photodetectors. Adv Mater 2010;22:3161–5.
[19] Pan ZW, Dai ZR, Wang ZL. Nanobelts of semiconducting oxides. Science 2001;291:1947–9.
[20] Xue J, Song J, Dong Y, et al. Nanowire-based transparent conductors for flexible electronics and optoelectronics. Sci Bull 2017;62:143–56.
[21] Deng K, Li L. CdS nanoscale photodetectors. Adv Mater 2014;26:2619–35.
[22] Wu PC, Ma RM, Liu C, et al. High-performance CdS nanobelt field-effect transistors with high-kappa HfO_2 top-gate dielectrics. J Mater Chem 2009;19:2125–30.
[23] Yang ZY, Wang DL, Meng C, et al. Broadly defining lasing wavelengths in single bandgap-graded semiconductor nanowires. Nano Lett 2014;14:3153–9.
[24] Li L, Lu H, Yang Z, et al. Bandgap-graded CdS_xSe_{1-x} nanowires for high-performance field-effect transistors and solar cells. Adv Mater 2013;25:1109–13.
[25] Zhou WC, Pan AL, Li Y, et al. Controllable fabrication of high-quality 6-fold symmetry-branched CdS nanostructures with ZnS nanowires as templates. J Phys Chem C 2008;112:9253–60.
[26] Wang YW, Meng GW, Zhang LD, et al. Catalytic growth of large-scale single-crystal CdS nanowires by physical evaporation and their photoluminescence. Chem Mater 2002;14:1773–7.
[27] Pan A, Yang H, Liu R, et al. Color-tunable photoluminescence of alloyed CdS_xSe_{1-x} nanobelts. J Am Chem Soc 2005;127:15692–3.
[28] Rose A. Concepts in photoconductivity and allied problems. New York: Interscience Publishers; 1963.
[29] Zhang F, Ding Y, Zhang Y, et al. Piezo-phototronic effect enhanced visible and ultraviolet photodetection using a ZnO-CdS core-shell micro/nanowire. ACS Nano 2012;6:9229–36.
[30] Xing X, Zhang Q, Huang Z, et al. Strain driven spectral broadening of Pb ion exchanged CdS nanowires. Small 2016;12:874–81.
[31] Zheng D, Fang H, Wang P, et al. High-performance ferroelectric polymer side-gated CdS nanowire ultraviolet photodetectors. Adv Funct Mater 2016;26:7690–6.
[32] Ye Y, Dai L, Wen XN, et al. High-performance single CdS nanobelt metal-semiconductor field-effect transistor-based photodetectors. ACS Appl Mater Interfaces 2010;2:2724–7.
[33] Gou GY, Dai GZ, Qian C, et al. High-performance ultraviolet photodetectors based on CdS/CdS:SnS_2 superlattice nanowires. Nanoscale 2016;8:14580–6.
[34] Shaygan M, Davami K, Kheirabi N, et al. Single-crystalline CdTe nanowire field effect transistors as nanowire-based photodetector. Phys Chem Chem Phys 2014;16:22687–93.
[35] Fan ZY, Ho JC, Jacobson ZA, et al. Large-scale, heterogeneous integration of nanowire arrays for image sensor circuitry. Proc Natl Acad Sci USA 2008;105:11066–70.
[36] Guo P, Hu W, Zhang Q, et al. Semiconductor alloy nanoribbon lateral heterostructures for high-performance photodetectors. Adv Mater 2014;26:2844–9.
[37] Li SY, Li XY, Zhao HP. Synthesis and electrical properties of p-type CdTe nanowires. Micro Nano Lett 2013;8:308–10.
[38] Gao T, Li Q, Wang T. CdS nanobelts as photoconductors. Appl Phys Lett 2005;86:173105.
[39] Li YB, Della Valle F, Simonnet M, et al. Competitive surface effects of oxygen and water on UV photoresponse of ZnO nanowires. Appl Phys Lett 2009;94:023110.
[40] Li QH, Gao T, Wang YG, et al. Adsorption and desorption of oxygen probed from ZnO nanowire films by photocurrent measurements. Appl Phys Lett 2005;86:123117.

Mingwei Tang received his Bachelor's degree in Optical Information Science and Engineering from Nanjing University of Science and Technology in 2016. He is current a Ph.D. student under the supervision of Prof. Qing Yang in the College of Optical Science and Engineering at Zhejiang University. His research focuses on the field of nanomaterials, metamaterials and their application in super-resolution imaging of biology.

Qing Yang received her Ph.D. degree in Materials Science and Engineering from Zhejiang University in 2006. She worked as a visiting scientist in Material Science and Engineering at Georgia Institute of Technology from 2009 to 2012. Currently, she is a Professor in the College of Optical Science and Engineering at Zhejiang University. Her research focuses on micro-/nanophotonics, piezo-phototronics and flexible nanosystems.